

Ferromagnetism in Oriented Graphite Samples

P. Esquinazi* and A. Setzer, R. Höhne, C. Semmelhack
*Department of Superconductivity and Magnetism, Institute for Experimental Physics II,
University of Leipzig, Linnéstr. 5, D-04103 Leipzig, Germany*

Y. Kopelevich
*Instituto de Física, Universidade Estadual de Campinas,
Unicamp 13083-970, Campinas, São Paulo, Brasil*

D. Spemann, T. Butz
*Department of Nuclear Solid State Physics,
Institute for Experimental Physics II, University of Leipzig,
Linnéstrasse 5, D-04103 Leipzig, Germany*

B. Kohlstrunk, M. Lösche
*Physics of Biomembranes,
Institute for Experimental Physics I, University of Leipzig,
Linnéstrasse 5, D-04103 Leipzig, Germany*
(Dated: October 24, 2018)

We have studied the magnetization of various, well characterized samples of highly oriented pyrolytic graphite (HOPG), Kish graphite and natural graphite to investigate the recently reported ferromagnetic-like signal and its possible relation to ferromagnetic impurities. The magnetization results obtained for HOPG samples for applied fields parallel to the graphene layers - to minimize the diamagnetic background - show no correlation with the magnetic impurity concentration. Our overall results suggest an intrinsic origin for the ferromagnetism found in graphite. We discuss possible origins of the ferromagnetic signal.

INTRODUCTION

We find in the literature reports on ferromagnetism in carbon-based compounds which apparently did not attract the necessary attention in the community. For example there are reports on ferromagnetic-like signals in pyrolytic carbon [1] and in HOPG [2]. In the first study pyrolytic carbon with higher crystallinity than usual was prepared from adamantane by chemical vapor deposition [1]. The metal impurities were claimed to be < 25 ppm and the ferromagnetic-like loop was reported to persist up to 400 K. In other work [2] the main study was the magnetization of Pd nanoparticles encapsulated in a graphite host. In the inset of their Fig. 2 the authors show a ferromagnetic-like hysteresis loop for graphite without Pd nanoparticles at a temperature of 300 K. We note that the saturation magnetization $M_s \sim 10^{-2}$ emu/g is much larger than the one measured in this work and by Kopelevich et al. [3]. Because the impurity concentration of that sample was not reported the origin of this signal remains, however, unclear. Amorphous-like carbon prepared by direct pyrolysis was found to be a stable strong magnet with a saturation magnetization comparable to magnetite [4]. The effect of the pyrolysis temperature on similar materials was also reported [5]. Ferromagnetism in pure C-60 induced by photo-assisted oxidation was reported to remain up to a critical temperature of 800 K, although the authors stated that only

a small part of the sample contributes to the ferromagnetism [6]. More recently, ferromagnetism in pure rhombohedral polymerized C-60 samples was reported to remain up to 500 K [7].

The recent report of ferromagnetic- and superconducting-like [3] magnetization hysteresis loops in HOPG in a broad temperature range opens several questions about the origin of the observed anomalies. Kopelevich et al. [3] found that the magnetization of HOPG samples shows ferromagnetic-like hysteresis loops up to 800 K. The details of the hysteresis depend on the sample, sample heat treatment and on the direction of the applied field. There has been a controversy between the opinion of the referees on the possible influence of impurities on the observations [3]. Therefore, more systematic work on the observed signal was necessary.

As clearly stated by J.S. Miller [8] for magnetic polymers, it appears that most of the claimed high-temperature ferromagnetism in nominally magnetic-ion free compounds in the past turned out to be of extrinsic origin. To establish that the low saturation magnetization of a material, as in the case of the reported HOPG ($M_s < 3\text{mG} = 3 \times 10^{-3}$ emu/cm³) might be of intrinsic origin, reproducibility and a quantification of extrinsic contributions must be achieved. Therefore and in order to clarify whether the observed ferromagnetism found in Ref. [3] reflects an intrinsic property of graphite or is due to ferromagnetic impurities, we have measured different

oriented graphite samples with different magnetic impurity concentrations (mainly Fe).

Both ferromagnetism and superconductivity have been predicted to arise in graphene layers in regions of certain topological defect structures [9]. On the other hand, ferromagnetic behavior due to edge states is also expected in graphene layers [10]. Taking into account all the experimental and theoretical work cited above we feel that a systematic study of the ferromagnetic-like hysteresis loops found in HOPG [3] as a function of magnetic impurities is necessary before speculating on its origin. Only a careful analysis of the data accompanied by a complete impurity concentration study on the same samples may provide an answer on the origin of the ferromagnetism found in HOPG.

The reported ferromagnetic-like signal was measured mostly for an applied field in direction parallel to the planes, whereas superconducting-like loops in HOPG were mainly observed with the magnetic field applied perpendicular to the planes after subtraction of the diamagnetic background [3]. This diamagnetic contribution depends strongly on the angle between applied field and the graphene layers reaching a minimum for the parallel orientation. Therefore, and in order to minimize any possible error due to the subtraction of the diamagnetic contribution, all the results reported in the current study were obtained with the field parallel to the graphene layers. With respect to the superconducting-like behavior observed in graphite [3] we would like to note that clear evidence for superconductivity in simple mixtures of graphite powder with sulphur has been reported recently [11].

The paper is organized as follows. In the next Section the samples characteristics and experimental details are given. In Section 3 we describe the results and in Section 4 we discuss the observed behavior and its possible origin. A short summary is given in Section 5.

SAMPLE CHARACTERISTICS AND EXPERIMENTAL DETAILS

Table I shows the magnetization characteristics, the impurity concentrations, the masses as well as the full width at half maximum (FWHM) of x-ray rocking curves in θ ($\Delta\theta$) and in 2θ ($\Delta(2\theta)$) of the measured graphite samples. Samples HOPG-2 and -3 were prepared at the Research Institute ‘‘Graphite’’ (Moscow) as described in Ref. [12]. Two commercial HOPG samples were from Union Carbide (samples UC3 and UC4, cut from the same batch) and Advanced Ceramics (samples AC1, batch 10158, and AC2, batch 25672). Furthermore, we have characterized a Kish and a natural graphite crystal, this last obtained from Ticonderoga (USA) [13].

The magnetization measurements were done with a Superconducting Quantum Interference Device (SQUID)

from Quantum Design with a 7 T superconducting solenoid. In general we have selected three cm scan length for the magnetization measurements. The SQUID response enables measurements of samples with a minimum magnetic moment $m \sim 3 \times 10^{-10} \text{ Am}^2$ ($3 \times 10^{-7} \text{ emu}$).

Because the magnetization signals of the samples are rather small we have checked the background signal from the sample holders in the SQUID. This contribution turned out to be non-negligible, and special care has been applied in the selection of the holder as well as with the sample handling procedure in order to prevent contamination of the holders and/or samples. For measurements below 350 K we have used a plastic tube with a small window and an adhesive tape (Tesa AG, Hamburg). The background signal of this sample holder with tape but without sample is shown in Fig. 1. Small but measurable hysteresis is observed which lies close to the resolution limit of our SQUID magnetometer. For measurements above 350 K the samples were fixed in a quartz tube between two quartz spacers and enclosed under a pressure of $2 \times 10^{-6} \text{ torr}$. The background signal in this case was negligible in comparison with the sample response.

In general, the ferromagnetic hysteresis is superimposed to a linear in field diamagnetic background. As noted above, this diamagnetic signal depends on the misalignment of the sample with respect to the field as well as on the intrinsic misalignment of the graphene planes in the sample. The diamagnetic contribution for each sample has been determined in-situ and in a straightforward way: Using a linear regression through the data points obtained for magnetic fields up to 5 T we obtained the diamagnetic slope $\chi_{||} = M(H)/H$. We note that the magnetization due to the superimposed ferromagnetic signal saturates at fields larger than 2 kOe and therefore it does not influence the linear field dependence of the diamagnetic background. The obtained susceptibility ranges between $0 \geq \chi_{||}(10K) \geq -5.3 \times 10^{-6} \text{ emu/gOe}$ for the studied samples. The ferromagnetic loop is then obtained from the measured magnetization $M(H)$ subtracting the diamagnetic background as $M(H) - \chi_{||}H$.

The crystallinity of the graphite samples was investigated by high resolution x-ray diffraction with a Philips X’pert diffractometer. θ and 2θ scans around the symmetrical (002) reflection were carried out using the Cu-K α 1 radiation. Furthermore, for three samples we have determined the average in-plane correlation length D from the 2θ scans around the symmetrical (110) reflection. As expected, D correlates with the FWHM obtained from the θ (002)-scans. Table I shows the FWHM of the 110 reflection as well as D for the samples AC2, HOPG-2 and HOPG-3.

The measurements of the impurity concentration were carried out with Particle Induced X-ray Emission (PIXE) using a 2 MeV proton beam. For the samples studied here the typical minimum detection limit (MDL) of this

method was $\leq 2\mu\text{g/g}$ (for some elements, much smaller). With exception of the natural graphite sample, the impurity concentration was distributed homogeneously in the samples. The concentration of all other magnetic elements not listed in Table I was less than $1\mu\text{g/g}$.

Scanning tunnelling microscopy (STM) was performed with a DI Nanoscope E in conjunction with a Small Sample scan head (“A” scanner, Digital Instruments, Santa Barbara, CA). Pt/Ir (80:20) tunneling tips (wire diameter: 0.25 mm) were from Plano (Wetzlar, Germany). Images were obtained under ambient conditions with a tip bias of typically +20 mV in the constant current-mode (scan rate $f = 3 \dots 6$ Hz; current $I_0 \approx 2$ nA) or in the constant height-mode (scan rate $f = 20 \dots 60$ Hz). While in both modes, a clear-cut discrimination of topology (height) differences from density-of-state (current) differences cannot be afforded, the first scanning mode emphasizes the topological structure whereas the latter accentuates local variations of the density of states.

RESULTS

Figures 2 to 4 show examples of the measured magnetization loops obtained in some of the samples at 300 K and 10 K. All HOPG samples show ferromagnetic-like hysteresis of the same order of magnitude. Figure 2 shows the hysteresis loops obtained for the samples from Advanced Ceramics at two different temperatures. Whereas the loop shown in (b) is obtained after subtraction of a diamagnetic background signal $\chi_{||} = -1.32 \times 10^{-6}$ emu/g Oe, the loop in (a) was obtained directly from the measurements without subtraction of any diamagnetic background. This result and the range of values obtained for $\chi_{||}$ suggest that the diamagnetic signal measured at high fields applied nominally parallel to the planes of HOPG samples is strongly influenced by the misalignment of the sample.

Figure 3 shows the loops obtained for two Union Carbide samples of different masses cut from the same batch. These results provide a measure of the typical scatter of the main values of the hysteresis loops in similar samples.

In order to check if there is any correlation of the hysteresis values with the measured Fe-concentration we plot in Figs. 5, 6 and 7 the remanent magnetization M_r , the magnetization at 2kOe $M(2\text{kOe})$ and the coercive field H_c , respectively, as a function of impurity content. From Fig. 5 one would tend to infer a weak increase of M_r with Fe concentration. However, the remanent magnetization is not the characteristic quantity that one expects to change systematically with Fe concentration since it depends primarily on the pinning of magnetic domains. Rather, a correlation of the saturation magnetization with the impurity content would be significant. Figure 6 shows that such a correlation is not observed within experimental error. A similar result is obtained

for the coercive field, see Fig. 7.

The FWHM obtained in θ and 2θ scans provides a measure of the variation in the orientation of a particular set of lattice planes (mosaic spread) and in the spacing of the graphene planes (e.g., inferred by dislocations), respectively. Figure 8 shows the magnetization at saturation as a function of $\Delta\theta$ (a) and $\Delta(2\theta)$ (b). We find no systematic dependence of $M(2\text{kOe})$ on $\Delta\theta$. A clear increase of $M(2\text{kOe})$ with $\Delta(2\theta)$ can be recognized in Fig. 8(b).

It has been reported [3] that annealing of HOPG samples leads to the disappearance of the superconducting-like hysteresis loop and turns it into a ferromagnetic-like loop. Also, short time annealing (~ 2 h) increases the ferromagnetic-like signal [3]. In the current work we have measured the hysteresis as a function of the annealing time and temperature. An increase of the ferromagnetic signal at the beginning of the annealing procedure was also observed in this work. Longer time annealing reduces however the ferromagnetic signal and reaches similar values as before the annealing. In Fig. 4(b) we show the data obtained at 300 K after annealing a different piece of the HOPG-2 sample for 16 h at 700 K (\circ) and additionally after 19 h at 800 K (\blacktriangle). The annealing procedure was done in situ in the SQUID under vacuum. It is observed that long time annealing has a weak influence, if any, on the hysteresis width and the saturation magnetization.

DISCUSSION

The origin of the ferromagnetic-like signal in HOPG samples is controversial. Therefore, we will discuss below different possible origins in view of the existing evidence.

(a) *Magnetic impurities.* The possibility of a significant contribution of magnetic impurities to the measured magnetic properties is taken serious and carefully analyzed before we discuss possible intrinsic origins of the hysteresis loops measured in graphite. In spite of the fact that no correlation between the observed magnetization and the Fe-concentration exists, one might still believe that those impurities are sufficient to produce the measured signals. A typical argument used to attribute a ferromagnetic signal to impurities would be as follows: Let us assume that all Fe impurities would form iron or magnetite (Fe_3O_4) clusters and that all clusters are large enough to behave ferro- or ferrimagnetically. An impurity content of $1\mu\text{g}$ Fe per gram graphite would then contribute $\simeq 2.2 \times 10^{-4}$ emu/g to the magnetization in the case of Fe clusters or $\simeq 1.4 \times 10^{-4}$ emu/g in the case of Fe_3O_4 clusters assuming that these clusters behave like bulk materials. Considering a linear increase of the magnetic moment with the Fe concentration, for most of the samples the possible contribution of the Fe impurities exceeds clearly the measured magnetization values at saturation or are on the same order of magnitude, see

Fig. 6. In the case of the Kish sample, AC2 and for HOPG-3 the measured values are larger than the maximum possible contribution from Fe clusters. Thus, for these three samples the values of magnetization cannot be explained by Fe impurities.

Moreover, the assumption that such a low Fe-concentration behaves ferromagnetically and produces a hysteresis loop with finite remanent moment and coercive fields at room temperature or even higher [3] is rather unlikely taking into account that the Fe concentration measured in the HOPG samples was found to be homogeneously distributed. To quantify the magnetization behavior of Fe impurities in graphite we have measured a natural graphite bulk sample that has an inhomogeneous Fe distribution through the sample between $13 \mu\text{g/g}$ and $3,790 \mu\text{g/g}$; most of the sample shows a concentration larger than $500 \mu\text{g/g}$ Fe. All other magnetic impurities are below $10 \mu\text{g/g}$ and may therefore be neglected. Figure 9(a) shows the hysteresis loop of the natural graphite crystal for fields parallel to its main plane after subtracting the paramagnetic (10 K) or diamagnetic (300 K) contributions (proportional to the applied field) shown in the inset. The measured hysteresis is very small with a remanent magnetization $M_r < 2 \times 10^{-5}$ emu/g. The magnetization at 2kOe is $< 4 \times 10^{-3}$ emu/g. Naively, one would argue that such a magnetization can be produced by $\sim 18 \mu\text{g/g}$ ferromagnetic Fe. Such a comparison is, however, misleading. If the magnetic signal is due to Fe impurities, the nearly negligible hysteresis width and the lack of saturation at 2 kOe indicate that Fe impurities do not behave ferromagnetically but rather superparamagnetically. To better understand this point we measured the magnetization up to 5 T and we obtained a ferromagnetic-like curve of negligible width, see Fig. 9(b), after subtracting the paramagnetic background contribution. We estimate that the saturation magnetization observed at 5 T is produced by $840 \mu\text{g/g}$ Fe, a concentration comparable to the average impurity content of the sample.

A typical response of superparamagnetic Fe in graphite is also recognized in the strong temperature dependence of the magnetization at 0.2 T below 150 K, see inset in Fig. 9(b). This behavior is in clear contrast to that obtained in the HOPG samples. As an example we show the temperature dependence of the magnetization measured at 2kOe in the HOPG-2 sample (after subtracting the diamagnetic contribution) in Fig. 10. It is recognized that the magnetization is practically temperature independent, in clear contrast to the expected behavior if the $8 \mu\text{g/g}$ of Fe would behave superparamagnetically. This result agrees with that reported in Ref. [3] that the saturation magnetization in annealed HOPG samples remains practically temperature independent up to 800 K. In line with that, the measured hysteresis loops for the HOPG-2 sample at 800 K (which is the highest possible in our equipment) indicate that the Curie temper-

ature is larger than that. From a linear extrapolation of the remanent magnetization (Fig. 10) to zero we estimate that the Curie temperature is of the order of 900 K. The small change observed in the hysteresis upon annealing the sample at 700 K or 800 K in vacuum, shown in Fig. 4(b), appears to be difficult to explain by arguing in terms of a magnetic contribution of ferrocene. From all the evidence presented here we believe that magnetic impurities can be excluded as the origin of the weak ferromagnetism observed in HOPG.

(b) *Topological defects: Grain boundaries and edge states.* The topological and electronic structure of atomically flat graphite surfaces has been extensively studied by scanning tunneling microscopy (STM) [14, 15, 16, 17]. More recently, the electronic properties of carbon nanotubes, and particularly edge states of nanometer-sized graphite ribbons, have attracted much interest [18, 19]. It is expected that the electronic structure of the graphite π system may differ considerably on carbons located within a graphite sheet and those at its edge [20, 21]. Moreover, such localized edge states have been shown to depend sensitively on the geometry of the edge [18]: While “zigzag” edges perpendicular to the $[1, 0, \bar{1}, 0]$ lattice direction show such states, “armchair” edges (perpendicular to $[1, 1, 2, 0]$) do not. Thus, “zigzag” edge states may lead to an increase of the density of states at the Fermi level. This has been experimentally confirmed in STM work on HOPG samples [19]. If such edge states occur at high density, a ferrimagnetic spin polarization may result. Experimental findings on graphitized nanodiamond [22] and activated carbon fibers [23] support this expectation. Similarly, a strong enhancement of the Curie-like paramagnetic contribution was predicted at low temperatures, see Ref. [10] and references therein, and this has been experimentally confirmed [24]. Recently, the mechanisms of magnetism in stacked nanographite were theoretically studied [25]. This work obtained an antiferromagnetic solution for A-B-type stacking only.

One may doubt that the edge states could be the origin for the ferromagnetism found in our macroscopic graphite samples, since in nanographites these states provide an enhanced paramagnetism and their size ~ 2 nm is smaller than the in-plane correlation length of our graphite samples (the influence of the edge states to the electronic properties of a graphene layer should decrease with D). However, small-size effects and the thermal energy could also preclude the formation of a stable ferromagnetic ordering in nanographite. It is also unclear whether correlation effects between edge states in macroscopic graphite samples with a in-plane correlation length not more than five times the size of the reported nanographite samples (see Table I) would not be enough to stabilize a ferromagnetic order. Theoretical studies suggest that the presence of strong topological disorder will stabilize ferromagnetism and frustate antiferromagnetic order [9]. No prediction was made, however, on the minimum density

of the disorder necessary for this situation. Therefore and because the theoretical results are not yet conclusive we should not neglect a possible contribution of edge states to stabilize the FM in bulk graphite.

In order to assess the role of edge states and their potential contribution to the magnetic properties of the graphite samples studied in this work, a systematic STM investigation of these samples would be desirable. Unfortunately, such a study is beyond the scope of our current experimental capabilities. In order to obtain at least a feeling whether or not edge states that might exist at grain boundaries within the graphite samples contribute to their observed anomalous magnetic properties we have conducted a limited study of some of the samples in air. We note that we are currently not capable of performing the spectroscopic studies [26] that were required to assess quantitatively putative differences in the density of states at the Fermi level as a function of the atom positions with respect to grain boundaries.

Figure 11 gives exemplary STM results obtained at a freshly cleaved surface of the HOPG-2 sample in air. The images have been flattened, but no filtering was applied to the raw data. Panel (a) shows a $125 \times 125 \text{ nm}^2$ surface topology overview observed in constant-current mode. Two types of linear defects are observed within the planar surface: A step line, oriented roughly along the scan direction (horizontal direction within the image) and an apparent elevation line that runs along the step defect at an oblique angle. Both line defects are much longer than the width of the image and are characterized in the section profile shown on the right. In other micrographs than the one shown in Fig. 11 we do not find indications that the two type of line defects are coupled to each other. By inspection of a large number of similar micrographs, we conclude that such defects are characteristic of the sample surface. On the surface of the HOPG-2 sample, they have a typical distance of a few 100 nm. Inspection of the unit cell orientations on both sides of the two types of defects at higher resolution (*vide infra*) reveals that both are associated with grain boundaries.

The section profile indicates that the step height of the first line defect is $\approx 0.65 \text{ nm}$, which corresponds to the length of one unit cell along the crystallographic \mathbf{c} axis, *i.e.* the height of two graphite sheets. In fact, an additional feature along the defect line at mid-level of the step is recognized. Since two stacked π rings in the unit cell are displaced sideways with respect to each other in the graphite crystal, this half-step may correspond to an individual graphite layer that protrudes laterally underneath the top layer. At a distance of a few nm from the step line, the profile is essentially flat. This is expected as the two planes correspond presumably to equivalent crystal surfaces that differ by one unit cell in height. However, as the trace on the higher level approaches the step, a pronounced steepening of the slope is observed. Since the

scan direction was chosen to be parallel to the step line, it cannot be argued that this feature is due to tip overshoot. Rather, because the experiment is inherently incapable of discriminating between topological features and changes of the density of states, the observed steepening of the contour line may more likely be associated with an increase of the local density of states on the carbon atoms as the topology approaches the grain boundary.

The apparent topology of the second line defect is distinctly different. The section profile registers a sharp, symmetric peak that has an apparent height, $\Delta z \approx 0.25 \text{ nm}$, and an apparent width of $\approx 2 \text{ nm}$. At higher resolution (Fig. 11(b), showing a constant-height scan of a similar defect on the same sample surface) the defect structure is disclosed in more detail. As recognized in the overview (inset) the defect line appears as three collinear stripes. These are no tip artifacts since they do not depend on the relative orientation between the defect line and the scan direction. The high resolution micrograph reveals that the corrugation is associated with individual surface atoms and that the lattice orientation differs on both sides of the central spine. The apparent height of the features with the highest elevations – truncated in the grey level scale which was chosen to better visualize the atomic lattice on the surrounding crystal faces – is about a factor of two larger than an atomic diameter. It is thus likely that an increase in the density of states on atoms near the grain boundary contribute to the appearance of these corrugations. Without a clean discrimination of topological and density-of-state features, however, it cannot in this case be decided with confidence whether or not the observed defects correspond simply to lines of atoms that decorate the grain boundary.

A high-resolution characterization of step-type line defects is presented in the lower half of Fig. 11. Panels (c) and (d) show the vicinity of the defect shown in Fig. 11 (a) at high resolution in constant-current and constant-height mode, respectively. The scan direction has been rotated by $\approx 90^\circ$ with respect to that in the overview scan. Similar to Fig. 11 (b), the images show the surface at atomic resolution. The fundamental corrugation is due to a carbon site asymmetry [14, 15] giving rise to a hexagonal lattice. Again, the constant-current micrograph – Fig. 11(c) – indicates a step height of $\Delta z \approx 0.6 \text{ nm}$ (section profile on the right). Both micrographs reveal clearly a misorientation of the lattices on both sides of the defect line of $42^\circ \pm 5^\circ$. On the higher level – to the left – the main lattice direction meets the grain boundary at $65^\circ \pm 5^\circ$, characteristic of a “zigzag” edge. By contrast, one would expect this angle to be 90° for an “armchair” edge. In distinction from an earlier report [19], where “zigzag” edges were observed to extend only for short lengths, the defects observed here may extend for $> 100 \text{ nm}$, as demonstrated in Fig. 11 (a) where the step defect runs along the same general direction over the entire, 125 nm , width of the micrograph.

In the close vicinity of the grain boundary itself, the constant-height image, Fig. 11 (d), appears distinctly different from the constant-current image. It is characterized by a vast overshooting of the section profile at the locations of the edge carbon atoms, *c.f.* pseudo-3D representation on the right of Fig. 11(d). While we reiterate that a clean distinction of topological and density-of-state features is not afforded in our measurements, we may note that the observed effect cannot easily be accounted for by the sample topology or elasticity effects [16]. For example, we consider it unrealistic that a decoration of the grain boundary with atoms (of an ordinary – low – density of states at the Fermi level) should be responsible for the observed giant corrugations. Rather, a large increase of the local density of states at the atom positions near the edge must be invoked to explain the observations. This is also hinted by the deviation of the section profile in the overview scan, Fig. 11 (a), from a planar topology near the step. The conjectured enhancement of the density of states on edge atoms may indicate the existence of a localized state as demonstrated in simulations [28]. Therefore, one may argue that topological defects such as the “zigzag” edge characterized in Fig. 11 affect the electronic properties of the bulk graphite crystal and might also be responsible, at least partially, for the measured ferromagnetic behavior. Clearly, a more definite conclusion on the importance of such localized states requires much more systematic STM work. In future, we are also planning to vary systematically the number of topological defects and thus quantify their influence on the magnetization. Preliminary results indicate indeed an increase of the ferromagnetic signal upon milling of a bulk sample.

Finally, we note that recent theoretical work points out the effects of the electron-electron interactions in a graphene layer suggesting the existence of both ferromagnetism and an anisotropic p -wave superconducting state [9]. This work also suggests that topological disorder in the graphene planes may enhance the electronic density of states and induce instabilities in the electronic system, thereby giving rise to the behavior reported here and in earlier work [3].

(c) *Itinerant ferromagnetism.* Since the carrier density in graphite is low, the magnetic properties may be connected to itinerant ferromagnetism of dilute two-dimensional electron gas systems when the electron-electron interaction is large. Indirect evidence for the importance of the electron-electron interaction in graphite has been recently obtained by magnetoresistance measurements that showed a field induced metal-insulator like transition with a scaling quantitatively similar to those found in MOSFET’s and amorphous thin films [29].

In general, the strength of the electron-electron interaction can be estimated through the Coulomb coupling

constant

$$r_s = \frac{1}{(\pi n_{2D})^{1/2} a_B^*}, \quad (1)$$

where the 2D carrier density is given by $n_{2D} = n_{3D}d$ with the interplane distance $d = 0.335$ nm, the effective Bohr radius $a_B^* = \epsilon \hbar^2 / e^2 m^*$, and the dielectric constant for graphite $\epsilon = 2.8$. The 3D carrier density of the majority band is $n_{3D} \simeq 2 \times 10^{18}$ cm⁻³ with an effective mass $m^* \sim 0.05 m_0$ where m_0 is the free electron mass. For the minority carriers, $n_{3D} \simeq 6 \times 10^{16}$ cm⁻³ with an effective mass $m^* \sim 0.004 m_0$ [30]. Substituting these values in eq. (1) we obtain $r_s \sim 5$ and ~ 10 for the majority and minority carriers, respectively. A value of r_s larger than 1 implies that the potential energy per electron is larger than the Fermi energy, hence effects due to the electron-electron interaction must be taken into account.

If we assume that Dirac fermions are responsible for the magnetic field driven metal-insulator-like transition in graphite (for fields parallel to the c -axis), the strength of the Coulomb coupling is characterized by the massless and dimensionless parameter [31, 32]

$$g = \frac{e^2}{\epsilon_0 v_F \hbar}, \quad (2)$$

where e is the electronic charge, ϵ_0 the dielectric constant and $v_F \sim 2 \times 10^6$ m/s the Fermi velocity for graphite. As noted recently [31], for graphite, $g > 10$ holds which suggests that the strong Coulomb interaction can open an excitonic gap in the spectrum of Dirac fermions. Interestingly, the occurrence of the gap is accompanied by the appearance of a small magnetic moment as the result of band anisotropy [31]. In agreement with this theory, conduction electron spin resonance (CESR) experiments performed in HOPG and Kish graphite samples reveal a ferromagnetic-like internal field [33]. It is expected that this doped excitonic FM would disappear above a certain level of doping of the order of the chemical potential [31]. We note that within this picture the excitonic gap and the nonzero spin polarization is driven by the Coulomb interaction even at zero magnetic field. On the other hand, a field applied normal to the graphene layers can induce the formation of a gap even when the Coulomb interaction is weak [31], a model used to interpret the recently found metal-insulator transition in HOPG [29].

It is also interesting to compare the magnetism found in graphite with that in the high-temperature itinerant $\text{Ca}_{1-x}\text{La}_x\text{B}_6$ ferromagnet [34] where either quantum localization effects [35] or an excitonic mechanism [36] are invoked to explain the observed weak ferromagnetism with a Curie temperature of 600 K. In graphite the low-temperature ferromagnetic magnetization at saturation is $\sim 1 \times 10^{-3}$ emu/g. This value can be translated in terms of the magnetic moment $\sim 0.1\mu_B$ per majority carrier similar to $0.07\mu_B$ found in $\text{Ca}_{1-x}\text{La}_x\text{B}_6$. Accord-

ing to Ref. [31] the ferromagnetism in graphite and hexaborides can have the same origin. Direct experimental evidence supporting an excitonic mechanism for the FM found in HOPG is, however, still lacking.

5. Summary

We have studied the magnetization of several HOPG, Kish graphite and natural graphite samples with different content of magnetic impurities. Our results rule out that ferromagnetic impurities can be responsible for the observed magnetic effects in HOPG and Kish graphite. The magnetization at saturation remains practically temperature-independent up to 500 K. This behavior is in clear contrast to that found in natural graphite samples with at least two orders of magnitude larger concentration of Fe-impurities. The results of natural graphite reveal the superparamagnetic behavior of Fe impurities in the carbon matrix. Long-time annealing at 700 K and 800 K in vacuum of the HOPG samples affects the hysteresis loops only weakly.

The origin of the FM in HOPG is not yet clear. We have discussed two possible origins in this work. Topological defects can contribute to the peculiarities of the graphite electronic properties and may give rise to ferromagnetic correlations. Also, the strong Coulomb interaction between electrons in graphite (due to the small electronic density) should play an important role in all the observed magnetic properties of graphite. However, details of the long-range itinerant ferromagnetic order remain unclear.

The discovery of ferromagnetism in oxidized C_{60} [6] as well as in polymerized rhombohedral C_{60} [7] indicates that carbon-based materials can be ferromagnetic without metallic components at high temperatures. Therefore, it should be no surprise if graphite itself shows weak ferromagnetic signals. Future work should try to (a) enhance the ferromagnetic signals by an appropriate mixing of graphite with other elements (an enhancement of the superconducting signal has been recently achieved mixing graphite with sulfur [11, 37]), (b) increase the defect concentration as well as (c) prove experimentally the existence of an excitonic gap.

We thank J. G. Rodrigo for the comments on our STM studies. This work is supported by the Deutsche Forschungsgemeinschaft within DFG Es 86/7-1. Y.K. was also supported by CNPq, FAPESP and CAPES. We acknowledge the support of the DAAD. M.L. is supported by the Fonds der Chemischen Industrie, Frankfurt.

* E-mail: esquin@physik.uni-leipzig.de

- [1] S. Mizogami, M. Mizutani, M. Fukuda, and K. Kawabata, *Synthetic Metals* **41-43**, 3271 (1991).
 [2] D. Mendoza, F. Morales, R. Escudero, and J. Walter, *J. Phys.: Condens. Matter* **11**, L317 (1999).

- [3] Y. Kopelevich, P. Esquinazi, J. H. S. Torres, and S. Moehlecke, *J. Low Temp. Phys.* **119**, 691 (2000).
 [4] K. Murata, H. Ushijima, H. Ueda, and K. Kawaguchi, *J. Chem. Soc.-Chem. Commun.* **7**, 567 (1992).
 [5] K. Murata and H. Ushijima, *J. Appl. Phys.* **79**, 978 (1996).
 [6] Y. Murakami and H. Suematsu, *Pure & Appl. Chem.* **68**, 1463 (1996).
 [7] T. Makarova et al. *Nature* **413**, 716 (2001).
 [8] J. S. Miller, *Adv. Materials* **4**, 298 (1992); *ibid* **4**, 435 (1992).
 [9] J. Gonzalez, F. Guinea, and M. Vozmediano, *Phys. Rev. B* **63**, 134421 (2001).
 [10] K. Wakabayashi, M. Fujita, H. Ajiki, and M. Sigrist, *Physica B* **280**, 388 (2000).
 [11] R. da Silva, H. Torres, and Y. Kopelevich, *Phys. Rev. Lett.* **87**, 147001 (2001).
 [12] N. B. Brandt, A. S. Kotosonov, S. V. Kuvshinnikov, and M. V. Semenov, *Sov. Phys. JETP* **52**, 476 (1980).
 [13] The crystal (collection Nr. 18154) was kindly provided by the Mineralogische Staatssammlung, Museum "Reich der Kristalle", München (Germany).
 [14] G. Binnig, H. Fuchs, Ch. Gerber, H. Rohrer, E. Stoll and E. Tosatti, *Europhys. Letters* **1**, 31 (1986).
 [15] S.-I. Park and C.F. Quate, *Appl. Phys. Letters* **48**, 112 (1986).
 [16] J.M. Soler, A. M. Baro, N. Garcia and H. Rohrer, *Phys. Rev. Letters* **57**, 444 (1986).
 [17] H. Fuchs and E. Tosatti, *Europhys. Letters* **3**, 745 (1987).
 [18] K. Nakada, M. Fujita, G. Dresselhaus G, and M.S. Dresselhaus, *Phys. Rev. B* **54**, 17954 (1996).
 [19] P. L. Giunta and S. P. Kelty, *J. Chem. Phys.* **114**, 1807 (2001).
 [20] M. Fujita, K. Wakabayashi, K. Nakada, and K. Kushakabe, *J. Phys. Soc. Jpn.* **65**, 1920 (1996).
 [21] M. Fujita, M. Igami, and K. Nakada, *J. Phys. Soc. Jpn.* **66**, 1864 (1997).
 [22] O. E. Andersson et al., *Phys. Rev. B* **58**, 16387 (1998).
 [23] A. Nakayama et al., *Synth. Met.* **57**, 3736 (1993).
 [24] Y. Shibayama, H. Sato, T. Enoki, and M. Endo, *Phys. Rev. Lett.* **84**, 1744 (2000).
 [25] K. J. Harigaya, *J. Phys.: Condens. Matter* **13**, 1295 (2001).
 [26] B. Reihl, J.K. Gimzewski, J.M. Nicholls and E. Tosatti, *Phys. Rev. B* **33**, 5770 (1986).
 [27] A. Krasheninnikov and V. F. Elesin, *cond-mat/9910498*.
 [28] K. Kobayashi, *Phys. Rev. B* **48**, 1757 (1993).
 [29] H. Kempa, Y. Kopelevich, F. Mrowka, A. Setzer, J. H. S. Torres, R. Höhne, and P. Esquinazi, *Solid State Commun.* **115**, 539 (2000).
 [30] M. S. Dresselhaus and G. Dresselhaus, *Adv. Phys.* **30**, 139 (1981).
 [31] D. V. Khveshchenko, *Phys. Rev. Lett.* **87**, 206401 (2001); *ibid* **87**, 246802 (2001).
 [32] Maria A. H. Vozmediano, M. Pilar Lopez Sancho, and F. Guinea, *cond-mat/0110418*.
 [33] M. S. Sercheli et al., *Solid State Commun.* **121**, 579 (2002).
 [34] D. P. Young et al., *Nature* **397**, 412 (1999).
 [35] D. M. Ceperly, *Nature* **397**, 386 (1999).
 [36] V. Barzykin and L. P. Gor'kov, *Phys. Rev. Lett.* **84**, 2207 (2000).
 [37] H. P. Yang, H. H. Wen, Z. W. Zhao, and S. L. Li, *Chin. Phys. Lett.* **18**, 1648 (2001), *cond-*

mat/0111445.

TABLE I: Characteristics of the investigated samples. The samples AC1, AC2, UC3, UC4, HOPG-2 and HOPG-3 are highly oriented pyrolytic graphite (see text), NG is a natural graphite crystal from Ticonderoga (USA) [13]. (a) All magnetization values are in units of 10^{-4} emu/g. The magnetization values in the table were obtained after subtraction of a linear background contribution. (b) The Fe concentration in this sample is not homogeneous. In four different position of the sample the Fe concentration was found to be between 0.10% and 0.38% (wt), in two other positions the values were between 13 $\mu\text{g/g}$ and 165 $\mu\text{g/g}$. (c) All impurity concentration values are in $\mu\text{g/g}$. For all samples the MDL ≤ 2 $\mu\text{g/g}$. n.d.: not determined.

Sample:	AC1	AC2	UC3/UC4	HOPG-2	HOPG-3	Kish	NG
mass (mg):	26.5	18.9	15.5/9.9	23.7	55.1	2.9	21.7
FWHM (θ ,002)	0.78°	0.401°	0.237°	1.33°	$0.60^\circ \pm 0.05^\circ$	$\sim 1.6^\circ$	5.05°
FWHM (2θ ,002)	0.124°	0.116°	0.119°	0.118°	0.22°	0.13°	-
FWHM (2θ ,110)	n.d.	0.966°	n.d.	2.08°	1.174°	n.d.	n.d.
D (nm)	n.d.	11	n.d.	5	9	n.d.	n.d.
$M(2\text{kOe},10\text{K})^{(a)}$	n.d.	2.7 ± 0.2	$5.6 \pm 0.4/12 \pm 2$	9.7 ± 1	25	10 ± 2	7.8 ± 0.2
$M(2\text{kOe},300\text{K})$	13.9	3.3 ± 0.4	$8.3 \pm 0.3/11 \pm 2$	9.3 ± 1	25	6 ± 2	-
$M_r(0, 300\text{K})$	3.58	0.5 ± 0.1	2.2/2.8	1.2 ± 0.2	1.77	0.7 ± 0.2	-
$H_c(10\text{K})$ (Oe)	n.d.	170 ± 30	$100 \pm 10/94 \pm 5$	105 ± 10	85 ± 2	170 ± 20	< 50
$H_c(300\text{K})(\text{Oe})$	98	70 ± 10	$70 \pm 5/65 \pm 10$	58 ± 4	60 ± 2	80 ± 2	-
Fe ^(c)	13 ± 1	< 0.3	16 ± 2	8 ± 2	7.8 ± 2	0.7 ± 0.3	(b)
Ni	1.3 ± 0.5	< 0.4	2.1 ± 0.7	0.8 ± 0.5	< 0.2	< 0.4	3 ± 2
Mn	< 0.3	< 0.3	< 0.2	< 0.2	< 0.2	< 0.3	10 ± 5
Cu	16 ± 2	< 0.5	73 ± 5	1.2 ± 0.5	1.3 ± 0.5	< 0.5	3 ± 2
Ca	< 0.7	< 0.7	56 ± 6	2.6 ± 0.8	9.7 ± 2.5	< 0.7	100 ± 30
Ti	9 ± 2	7 ± 1	3.3 ± 1	0.8 ± 0.5	1.0 ± 0.7	< 0.5	< 1

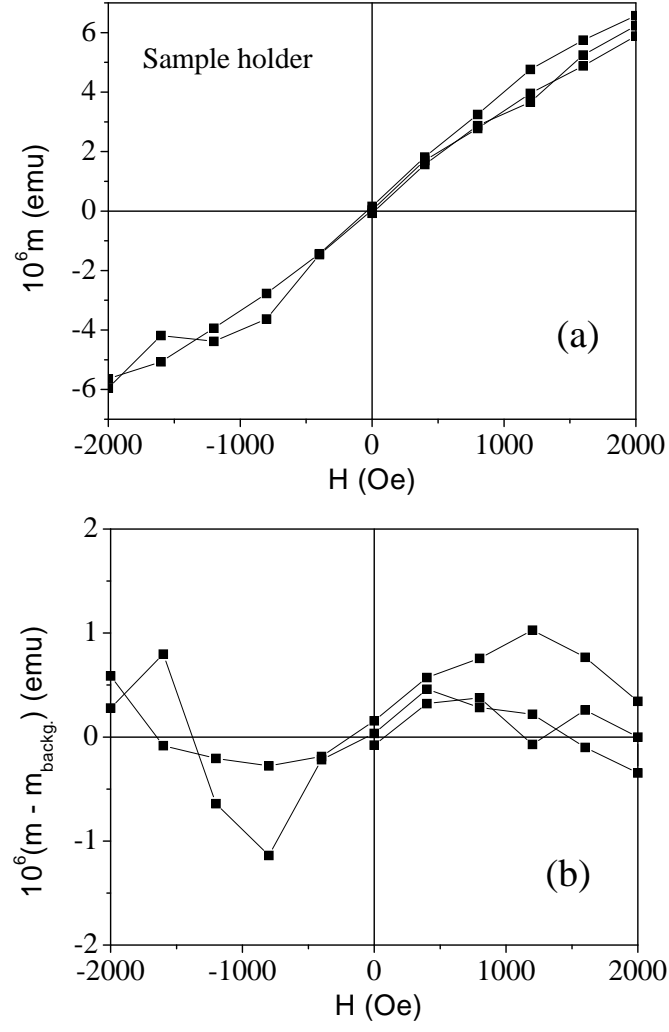


FIG. 1: (a) Magnetic moment of the sample holder (plastic tube with a small window and an adhesive tape) as a function of applied field at $T = 10$ K. (b) The results from (a) after subtraction of the linear paramagnetic background. $1 \text{ emu/g} = 1 \text{ A m}^2 / \text{kg}$, $1 \text{ Oe} = 10^3/4\pi \text{ A/m}$.

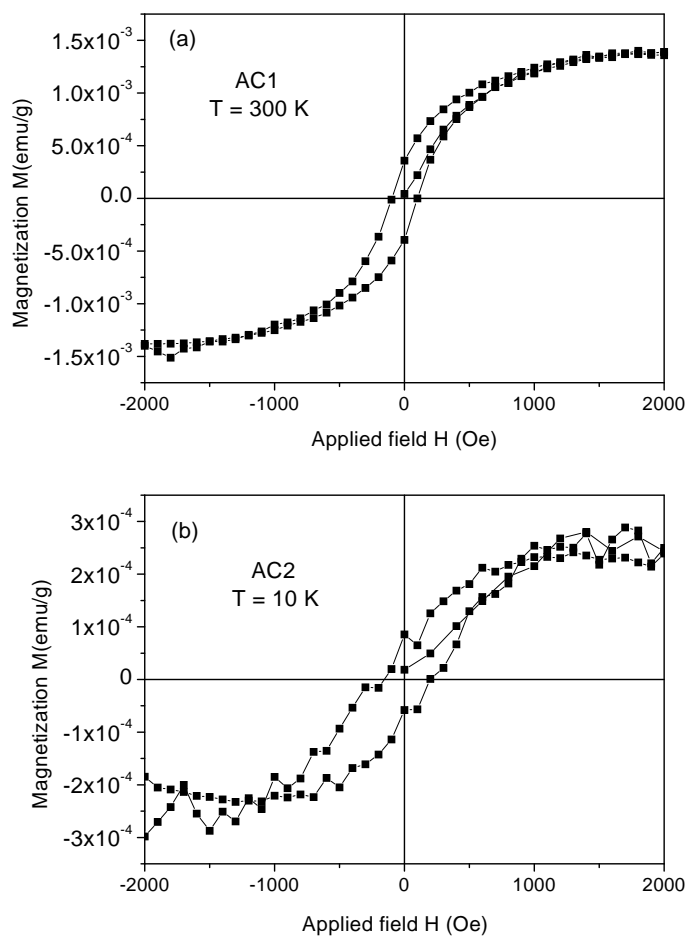


FIG. 2: (a) Magnetization as a function of applied field at $T = 300$ K for sample AC1. No background subtraction has been performed. (b) The same for sample AC2 at 10 K after subtraction of a diamagnetic background, $\chi = -1.32 \times 10^{-6}$ emu/g Oe. The sample holder background (see Fig. 1) was not subtracted from the data.

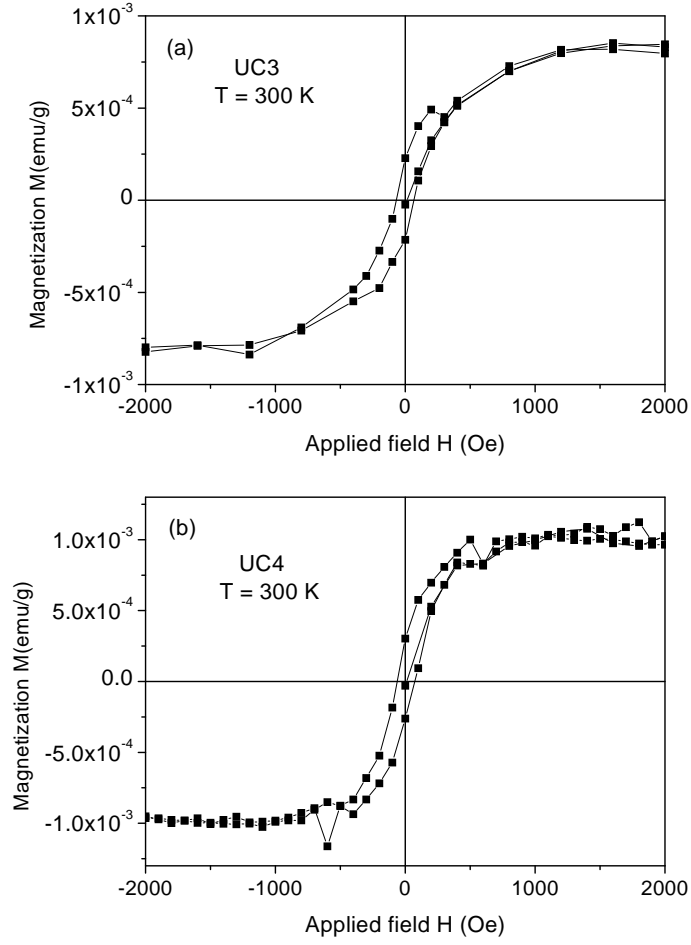


FIG. 3: (a) Magnetization as a function of applied field at $T = 300$ K for sample UC3 (Union Carbide). A diamagnetic background $\chi = -2.58 \times 10^{-6}$ emu/g Oe has been subtracted. (b) The same for sample UC4 at 300 K after subtraction of a diamagnetic background $\chi = -1.74 \times 10^{-6}$ emu/g Oe.

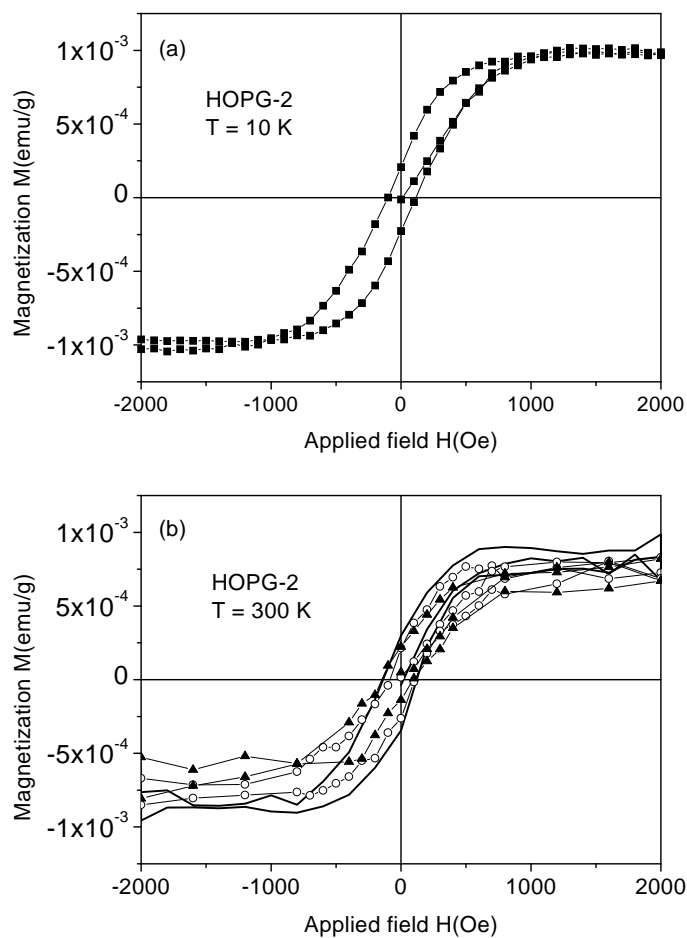


FIG. 4: (a) Magnetization as a function of applied field at $T = 10$ K for sample HOPG-2. (b) Similar plot for a different piece of the same sample at 300 K after annealing in vacuum at a temperature of 700 K for 16 h (\circ) and after 19 h at 800 K (\blacktriangle). The bold line represents the hysteresis at the same temperature before annealing. A diamagnetic background has been subtracted.

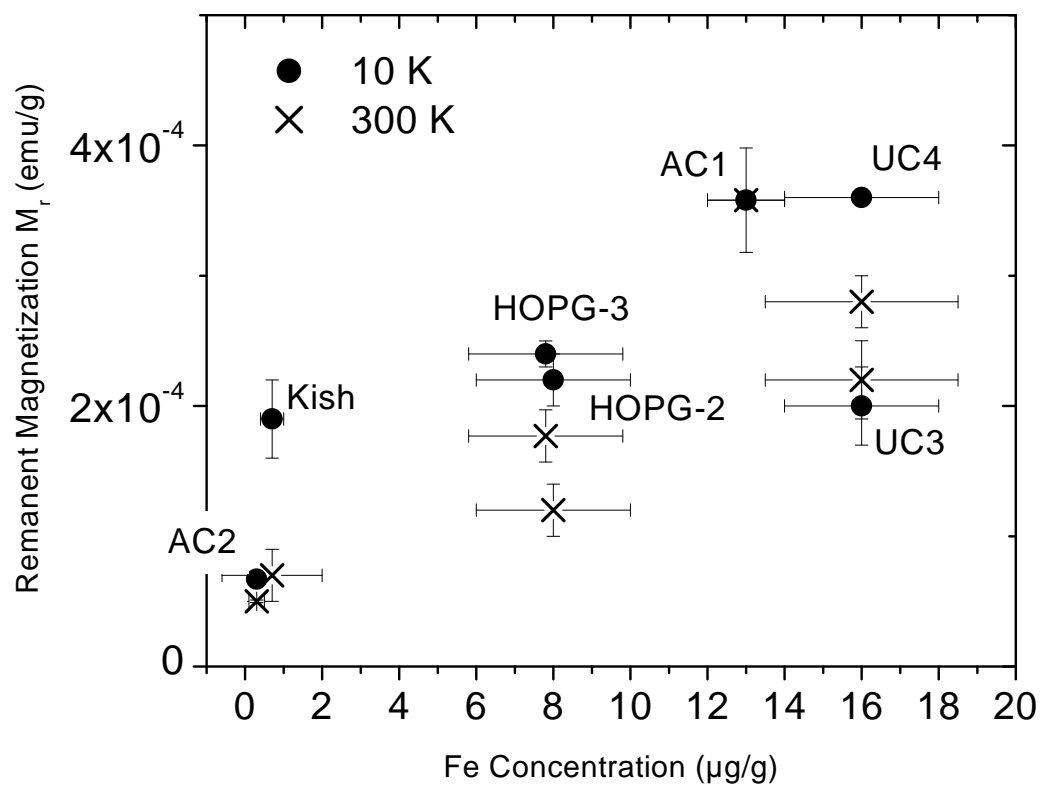


FIG. 5: Remanent magnetization as a function of Fe concentration at two temperatures of all HOPG and Kish graphite samples.

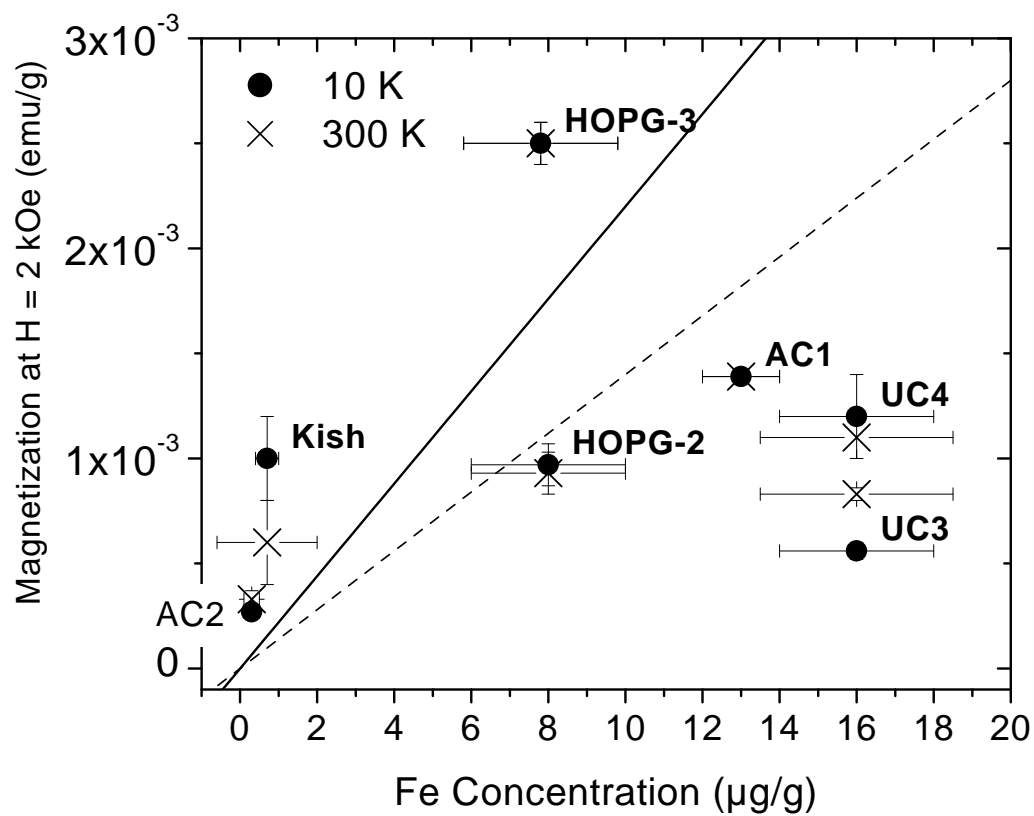


FIG. 6: Magnetization at 2 kOe as a function of Fe concentration at two temperatures of HOPG and Kish graphite samples. The solid line represents the expected magnetization if Fe contained in the samples was in a ferromagnetic state. The dashed line represents a similar relation for Fe_3O_4 .

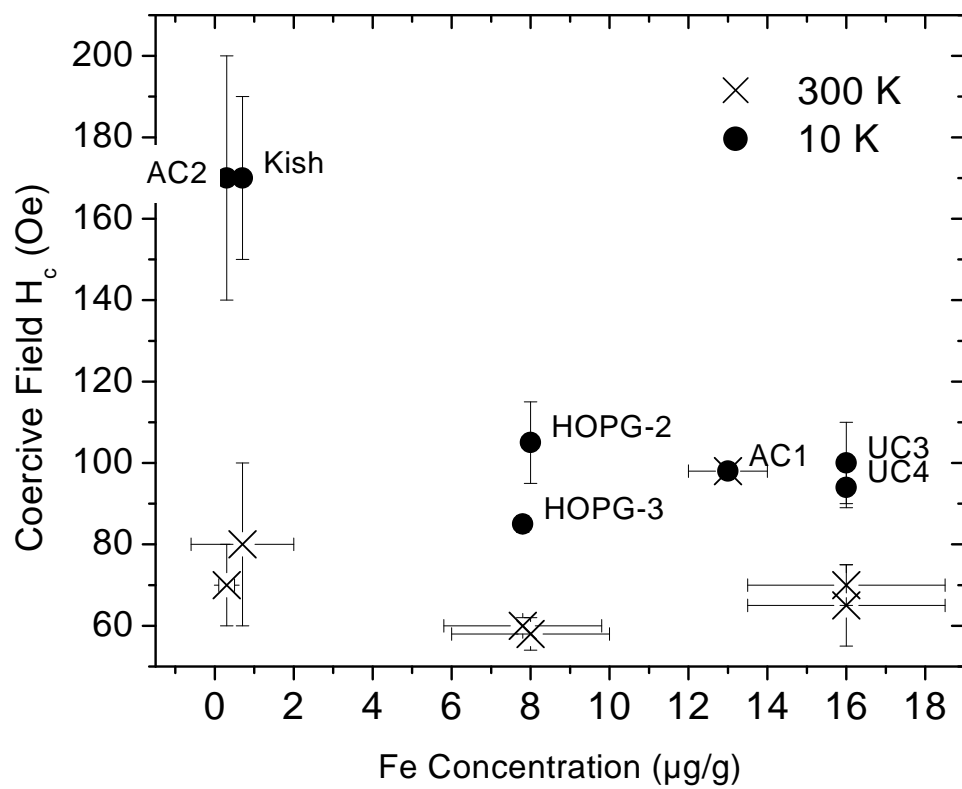


FIG. 7: Coercive field at two temperatures of the HOPG and Kish graphite samples as a function of Fe concentration.

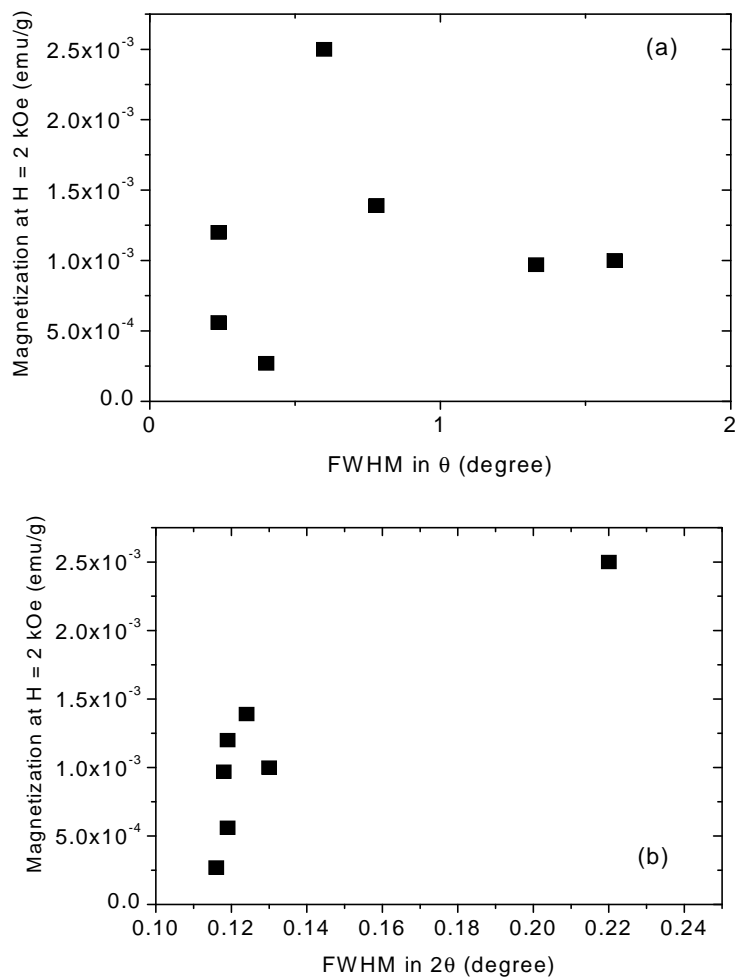


FIG. 8: (a) Magnetization at 2kOe ($T = 10 \text{ K}$) as a function of the full width at half maximum (FWHM) in θ for all HOPG and Kish graphite samples. (b) Similar plot as a function of the FWHM in 2θ .

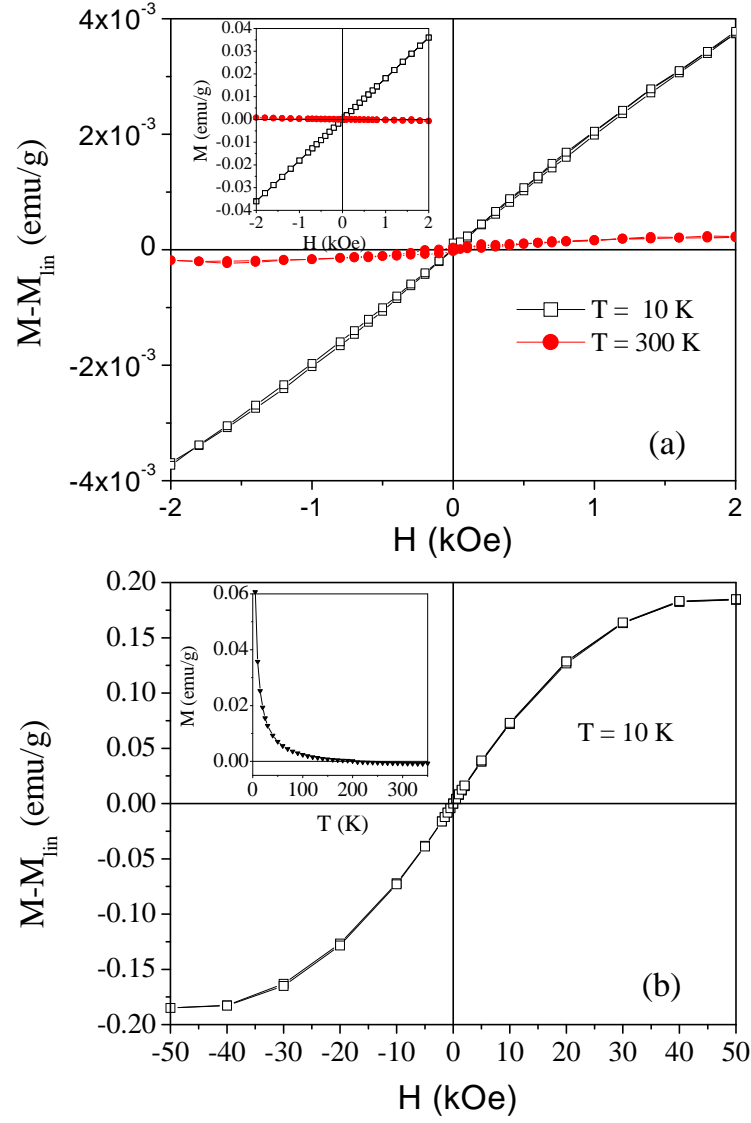


FIG. 9: (a) Magnetization as a function of applied field at 10 K and 300 K for the natural graphite crystal with an average Fe-concentration of more than $500 \mu\text{g/g}$. A linear background contribution was subtracted. These are shown in the inset. (b) Similar plot at 10 K and up to ± 50 kOe applied field. The inset shows the temperature dependence of the magnetization at 2 kOe.

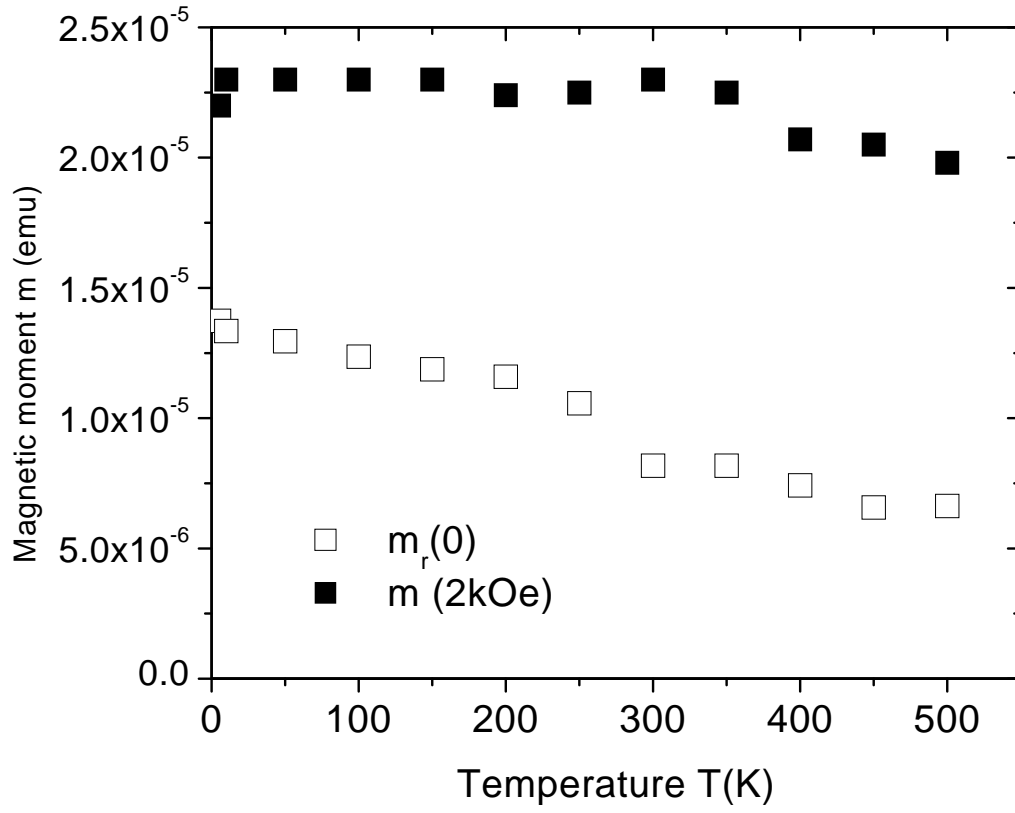


FIG. 10: Temperature dependence of the saturation (■) and remanence (□) magnetic moment for the sample HOPG-2 after annealing 16 h at 700 K. In the present work and due to technical reasons we were not able to measure $M(T)$ continuously up to 800 K.

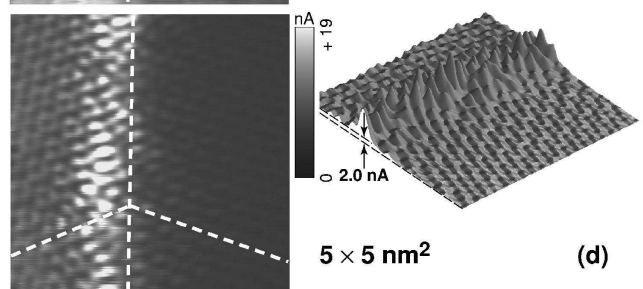
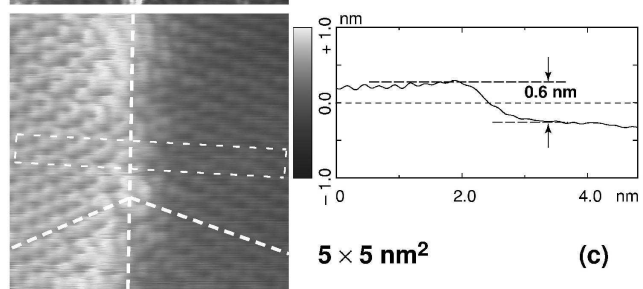
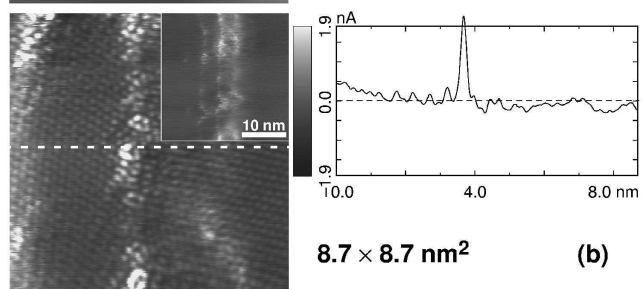
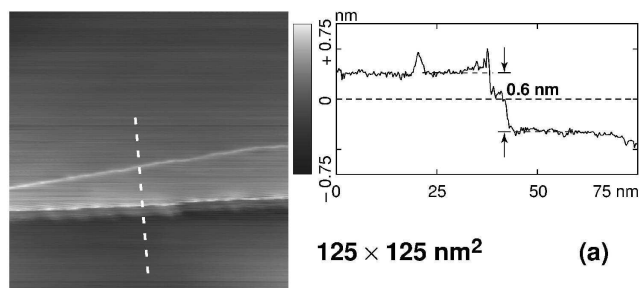


FIG. 11: STM images of a freshly cleaved surface of the sample, HOPG-2, in air (left) and their analysis using section profiles (right). The ordinate scales in (a) – (c) apply to both the section profiles and the grey scales. (a) Overview scan in constant-current mode ($V_t = 32$ mV, $I_0 = 1.25$ nA, $f = 6$ Hz). In the section profile determined along the dashed line (right), a linear ramp has been subtracted to emphasize the flatness of the plateaus. (Thus, the profile levels do not entirely faithfully correspond to the grey levels shown in the micrograph.) Close to the step line that is recognized in the lower third of the image, an increase of the slope of the section profile is observed. Correcting for this overshoot, a step height of ≈ 0.6 nm is determined. (b) High-resolution constant-height image and cross-section ($V_t = 33.5$ mV, $I_0 = 1.0$ nA, $f = 27.5$ Hz) of a surface region incorporating a line defect similar to the one shown in panel (a) “north” of the step defect. Atomic resolution is achieved within the planar sections of the sample surface and indicates that the line defect corresponds to a boundary between differently oriented grains. The inset in the micrograph shows a constant-current ($V_t = 33.5$ mV, $I_0 = 1.0$ nA, $f = 2.0$ Hz) overview of the same surface feature. Scan size here is 25.4×25.4 nm². The grey scale of the overview is distinct from that of the main image and ranges from 0 to 1.0 nm (black to white). (c) and (d) Constant-current ($V_t = 20$ mV, $I_0 = 2.0$ nA, $f = 2.9$ Hz) and constant-height ($V_t = 20$ mV, $I_0 = 2.0$ nA, $f = 55$ Hz) images, respectively, of the step defect shown in panel (a). The scan direction has been rotated by 90° with respect to that in the overview scan. The section profile in (c) has been determined in the rectangle bounded by thin dashed lines. Fat dashed lines indicate the grain boundary as well as the prevalent lattice directions within the grains near the boundary. In panel (d), the image is dominated by giant corrugations at atom sites immediately at the boundary. The relative proportions of these corrugations with respect to the amplitudes observed further away from the defect line is more clearly revealed in the pseudo-3D plot shown on the right.